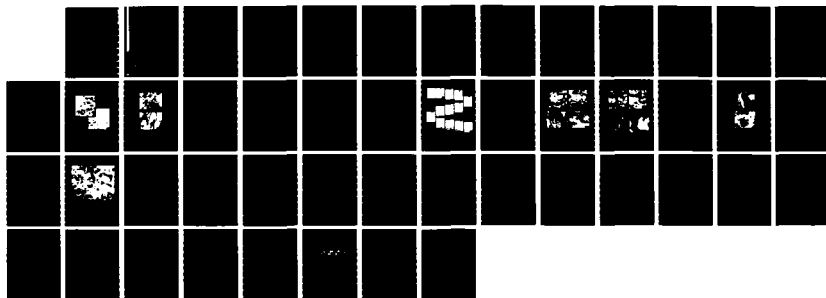MICROMECHANISMS OF CRACK GROWTH AND FRACTURE TOUGHNESS
IN METAL MATRIX COMPOSITES(U) SOUTHWEST RESEARCH INST
SAN ANTONIO TX   D L DAVIDSON ET AL. JUN 86 SWRI-06-8602

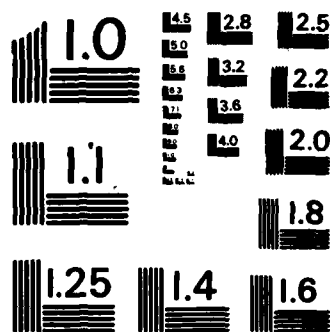MICROCOPY RESOLUTION TEST CHART

NATIONAL BUREAU OF STANDARDS-1963-A

06-8602/1

⑫

MICROMECHANISMS OF CRACK GROWTH AND FRACTURE TOUGHNESS IN METAL MATRIX COMPOSITES
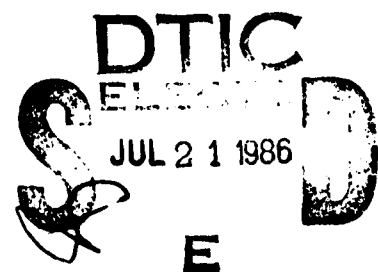
Technical Report for the Period 4/29/85 to 4/29/86

Prepared For

Office of Naval Research
800 North Quincy St.
Arlington, VA 22217

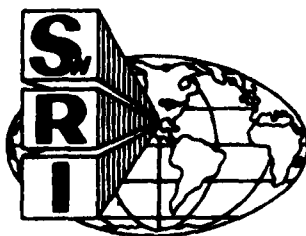By D. L. Davidson, J. Lankford and G. R. Leverant

Southwest Research Institute
P. O. Box 28510
San Antonio, TX 78284

DTIC
S E L E C T E D
JUL 2 1 1986
E

June 1986

SOUTHWEST RESEARCH INSTITUTE
SAN ANTONIO   HOUSTON

86 7 18 006

A169839   12

REPORT DOCUMENTATION PAGE

1a. REPORT SECURITY CLASSIFICATION	1b. RESTRICTIVE MARKINGS
Unclassified	

2a. SECURITY CLASSIFICATION AUTHORITY	3. DISTRIBUTION/AVAILABILITY OF REPORT
2b. DECLASSIFICATION/DOWNGRADING SCHEDULE	Unlimited

4. PERFORMING ORGANIZATION REPORT NUMBER(S)	5. MONITORING ORGANIZATION REPORT NUMBER(S)
06-8602	NR 039-283

6a. NAME OF PERFORMING ORGANIZATION	6b. OFFICE SYMBOL (If applicable)	7a. NAME OF MONITORING ORGANIZATION
Southwest Research Institute		Dr. Steven G. Fishman - Code 431N Office of Naval Research

6c. ADDRESS (City, State and ZIP Code)	7b. ADDRESS (City, State and ZIP Code)
6220 Culebra Road San Antonio, TX 78284	800 North Quincy Street Arlington, VA 22217-5000

8a. NAME OF FUNDING/SPONSORING ORGANIZATION	8b. OFFICE SYMBOL (If applicable)	9. PROCUREMENT INSTRUMENT IDENTIFICATION NUMBER
Office of Naval Research		N00014-85-C-0206

8c. ADDRESS (City, State and ZIP Code)	10. SOURCE OF FUNDING NOS.			
800 North Quincy Street Arlington, VA 22217-5000	PROGRAM ELEMENT NO.	PROJECT NO.	TASK NO.	WORK UNIT NO.

11. TITLE (Include Security Classification) Micromechanisms of Crack Growth and Fracture Toughness in Metal Matrix Composites

12. PERSONAL AUTHOR(S) D. L. Davidson, J. Lankford and G. R. Leverant

13a. TYPE OF REPORT	13b. TIME COVERED	14. DATE OF REPORT (Yr., Mo., Day)	15. PAGE COUNT
Technical	FROM 4/29/85 TO 4/29/86	June 1986	

16. SUPPLEMENTARY NOTATION

Square root of M Cubed

17. COSATI CODES			18. SUBJECT TERMS (Continue on reverse if necessary and identify by block number) Key Words
FIELD	GROUP	SUB. GR.	Metal matrix composites, silicon carbide reinforcement, mechanical alloying, fatigue crack growth, fracture toughness, particulate strengthening, crack growth micromechanisms

19. ABSTRACT (Continue on reverse if necessary and identify by block number)

Subcritical crack growth and rapid fracture of the mechanically alloyed aluminum alloy IN-9052 reinforced with SiC particles have been investigated. Fatigue crack growth rates for the composite exceed those of the unreinforced alloy, except that the threshold stress intensity for growth is higher for the composite. Fracture toughness of the composite is about 9 $MN/m^{3/2}$ compared to a (reported) value of 29 $MN/m^{3/2}$ for the unreinforced alloy. The contributions to fracture toughness from work done within the plastic zone and in formation of the void sheet have been computed using analytical models. Fracture toughness is shown to result almost entirely from work done within the plastic zone of the growing crack. The matrix microstructure and the particulate characteristics are found to account for the elastic and fracture properties of this composite.

DTIC JUL 21 1986

20. DISTRIBUTION/AVAILABILITY OF ABSTRACT	21. ABSTRACT SECURITY CLASSIFICATION
UNCLASSIFIED/UNLIMITED ☐ SAME AS RPT. ☒ DTIC USERS ☐	Unclassified

22a. NAME OF RESPONSIBLE INDIVIDUAL	22b. TELEPHONE NUMBER (Include Area Code)	22c. OFFICE SYMBOL
David L. Davidson	512/522-2314	E

DD FORM 1473, 83 APR   EDITION OF 1 JAN 73 IS OBSOLETE.

TABLE OF CONTENTS

TABLE OF CONTENTS (CONTINUED)

Accession For

NTIS   &I

DTIC T

Unan...   d

Justifi. tion.

By

Distribution/

Availability Codes

Dist	Avail and/or Special
A-1	

QUALITY INSPECTED 1

LIST OF ILLUSTRATIONS

iv

FRACTURE CHARACTERISTICS OF Al-4%Mg
MECHANICALLY ALLOYED WITH SiC

Abstract

Subcritical crack growth and rapid fracture of the mechanically alloyed aluminum alloy IN-9052 reinforced with SiC particles have been investigated. Fatigue crack growth rates for the composite exceed those of the unreinforced alloy, except that the threshold stress intensity for growth is higher for the composite. Fracture toughness of the composite is about 9 $MN/m^{3/2}$ compared to a (reported) value of 29 $MN/m^{3/2}$ for the unreinforced alloy. The contributions to fracture toughness from work done within the plastic zone and in formation of the void sheet have been computed using analytical models. Fracture toughness is shown to result almost entirely from work done within the plastic zone of the growing crack. The matrix microstructure and the particulate characteristics are found to account for the elastic and fracture properties of this composite.

INTRODUCTION

Aluminum alloys reinforced with silicon carbide particles show an increased modulus, due to the higher modulus of the silicon carbide, and often exhibit an increased flow stress, depending on the matrix alloy and

its treatment in the manufacturing process and any subsequent heat treatment given the composite. Three manufacturing processes are currently used for manufacturing these composites: (1) silicon carbide is mixed with a molten aluminum alloy, which is subsequently cast and, perhaps further worked, (2) silicon carbide is mixed with rapidly solidified aluminum alloy powder, which is then consolidated into a billet using powder metallurgy forming processes, and (3) mechanically alloyed aluminum alloy powders are mechanically "alloyed", or mixed, with silicon carbide and formed using P/M manufacturing methods. Each of these processes results in composites with different properties, and it is not known if this due solely to the manufacturing process or if there are other causes, such as the size and distribution of the silicon carbide particles.

Although these composites show increases in modulus and yield strength, they have values of fracture toughness less than unreinforced alloys and lower than desirable for many structural uses. The research reported here was undertaken to examine the origins of low fracture toughness in these composites, and to suggest ways of increasing this property. Composites made by all manufacturing processes, and having approximately equal volume fractions of silicon carbide are being studied. This paper reports on our investigation of the mechanically alloyed, powder metallurgy product designated as IN-9052 containing 15 volume percent SiC manufactured by the NOVAMET subsidiary of International Nickel Company. Composition of the matrix material was given as follows (1): Al-4Mg-1C-.90 (wt.%). Similar results will be published later for composites formed by other processes.

The goals of this work were to measure the physical and chemical characteristics of this material, and determine how these factors control mechanical properties of the composite, especially fracture. Both fatigue and fracture toughness were studied, and a method was devised for computing the fracture toughness from measured physical properties.

MECHANICAL CHARACTERISTICS

1.   Fatigue and Fracture Toughness:

Two single edge notched specimens 19 x 2.8 mm were machined from an as-received extrusion of cross section 44 x 9.5 mm and metallurgically prepared. The specimens were cycled at a stress ratio (R) of 0.1 until a crack initiated and grew away from the influence of the notch. Load was slowly reduced until crack growth was below 10^{-8} meters/cycle, and then it was slowly increased. Periodically, the specimen was removed from the laboratory loading frame and inserted into a special cyclic loading stage for the scanning electron microscope, which allows dynamic observation of the crack tip under high resolution conditions with good depth of field. The specimen was cycled in the SEM and the crack tip was periodically photographed in both the loaded and unloaded condition. Thus, the path of the fatigue crack through the composite was traced and recorded with increasing stress intensity until the point of instability was reached, leading to rapid fracture. Load at this point was used to compute fracture toughness, K_{IC}. For the two specimens tested, K_{IC} = 8.9 ± 0.2 $MN/m^{3/2}$.

Measured fatigue crack growth rates are shown in Fig. 1, and, as indicated, this curve terminates with the fracture toughness value. Crack growth data from both specimens agreed very well. These data were fit by the least squares method using the equation

$$^{da}/dN = B\Delta K_{eff}^{\ s} \tag{1}$$

where $B = 1.92 \times 10^{-8}$ m/cy and $s = 1.59$, and $\Delta K_{eff} = \Delta K - \Delta K_{TH}$. The value derived for $\Delta K_{TH} = 4.05$ MN/m$^{3/2}$. If a straight line is fit through the data, $B = 1.1 \times 10^{-12}$ m/cy and $s = 5.99$.

2. Tensile Properties:

Stress-strain curves of this material were made at a displacement rate of 1.2 mm/minute. A curve of continuous loading, shown in Fig. 2, fits the equation

$$\sigma = \sigma_y(\epsilon/\epsilon_y)^n \tag{2}$$

where σ and σ_y = stress and yield stress, and ϵ and ϵ_y = strain and yield strain, respectively. This equation may be integrated to give the work done in deforming the specimen to the strain e_t:

$$W_t = \frac{\sigma_y \epsilon_y}{n+1} \left(^{\epsilon_t}/\epsilon_y\right)^{n+1} = W_0 \epsilon_t^{\ m} \tag{3}$$

By computing the work beneath the stress-strain curve and plotting it against strain, W_0 and m may be derived. The values determined from the stress strain curve of Fig. 2 are given in Table 1. Since Hooke's Law relates σ_y and ϵ_y, independent choice of both σ_y and E is not allowed by Eq. (3). Thus, a second stress-strain specimen was tested in which a periodic
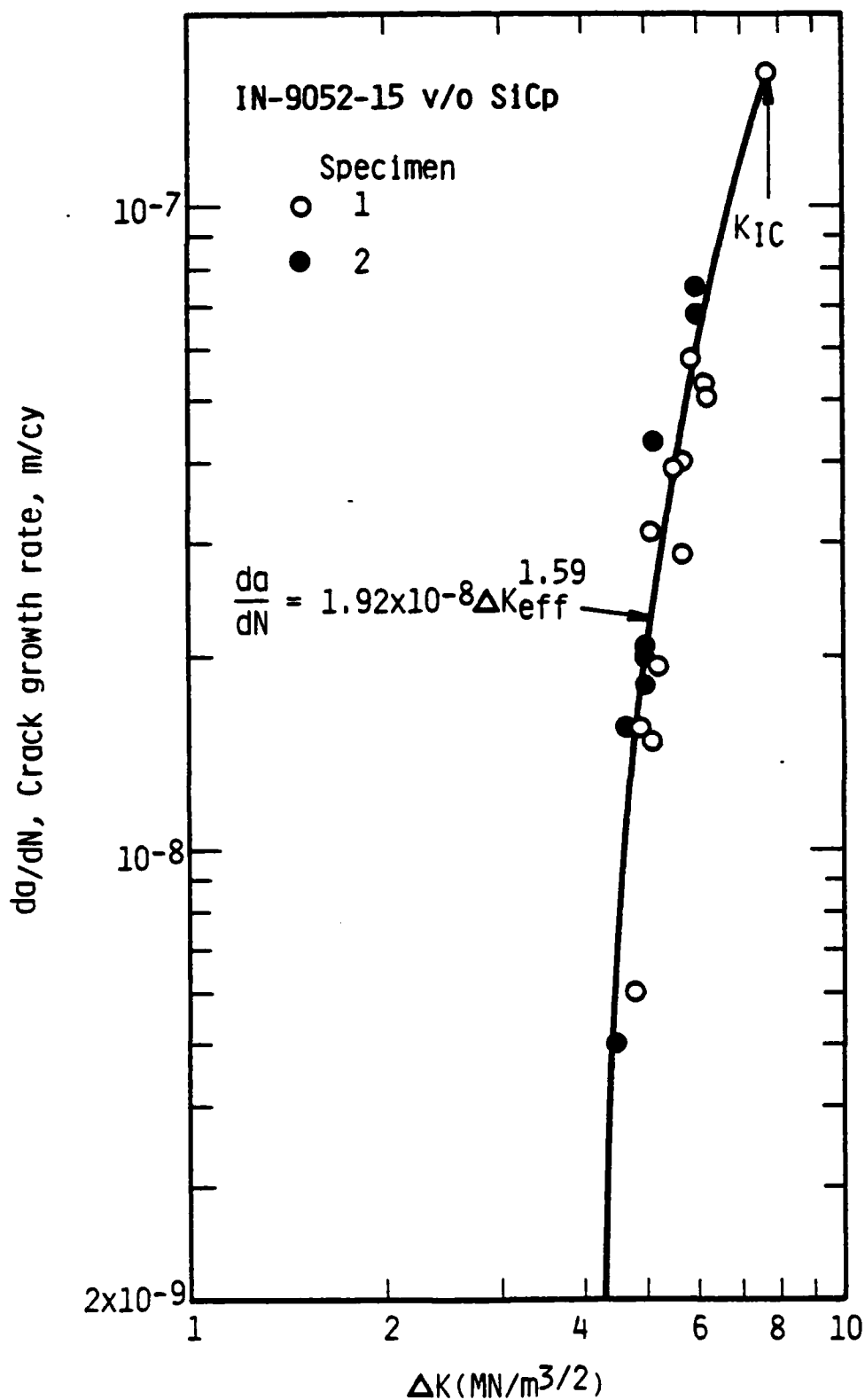
Figure 1. Composite fatigue crack growth rate. Data were collected from two single-edge notched specimens. Curve through data was fit using least-squares procedure assuming that $\Delta K_{eff} = \Delta K - \Delta K_{TH}$. Derived values of $\Delta K_{TH} = 4.05$ MN/m$^{3/2}$.
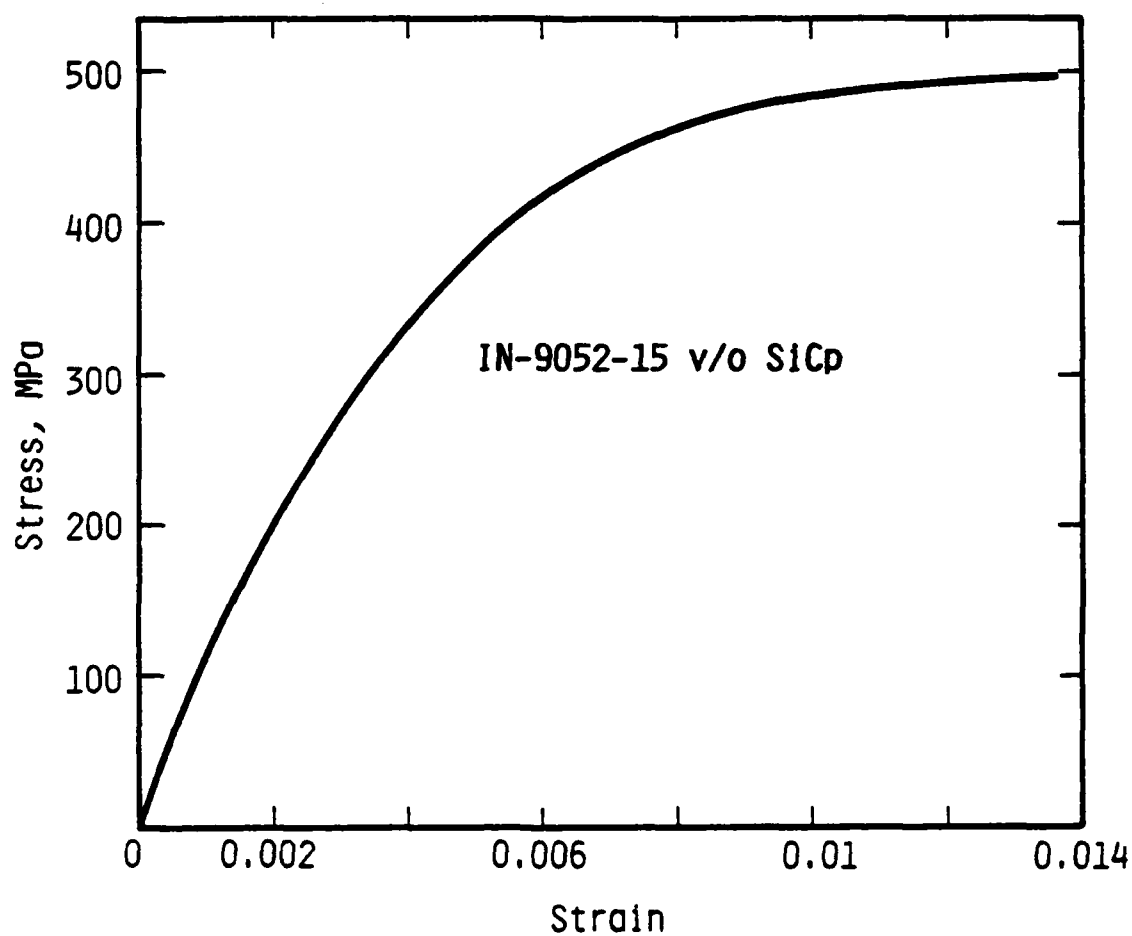
Figure 2. Tensile stress-strain curve showing parabolic shape with undefined proportional limit and modulus.

TABLE 1

IN-9052 + 15 v/o SiC
Mechanical Properties

Fatigue crack growth curve: $B = 1.92 \times 10^{-8}$ m/cy, $s = 1.59$, $\Delta K_{TH} = 4.05$ MN/m$^{3/2}$

Fracture toughness: $K_{Ic} = 8.9 \pm 0.2$ MN/m$^{3/2}$

$E = 8.4 \times 10^4$ MPa $\qquad$ $\sigma_y = 280$ MPa $\qquad$ $\sigma_{.02\%} = 450$ MPa

$W_o = 5.4 \times 10^3$ MPa $\qquad$ $\sigma_u = 495\text{-}518$ MPa $\qquad$ $\varepsilon_f = .013\text{-}.023$

$m = 1.6$

Matrix: $\qquad$ $\sigma_y = 550$ MPa $\qquad$ $\sigma_u = 580$ MPa $\qquad$ $\varepsilon_f = .08$ (Ref. 12)
(Ref. 12) $\qquad$ $K_Q = 29$ MN/m$^{3/2}$

unloading cycle was included to measure the modulus and proportional limit. The value of modulus determined in this way was E = 84 GPa, and the associated yield stress computed using Eq. (3) is 280 MPa. Other values determined from the stress strain curve are listed in Table 1. Computing modulus using the Voight averaging method (rule of mixtures) gives E = 116 GPa, while by the Reuss averaging technique gives E = 80 GPa, the latter value being only 5% lower than that measured (using E_{SiC} = 470 GPa).

PHYSICAL CHARACTERIZATION

1.   Particle Size Distribution:

A typical distribution of SiC particles is shown in the SEM micrograph of Fig. 3, which, has a resolution limit of about 0.05 μm. Transmission electron microscopy (TEM) was also used to examine the finer structure of the matrix. It was necessary to use a dimpling device in order to obtain transparent foils of this difficult to thin material. TEM micrographs of the matrix parallel to the extrusion direction are shown in Fig. 4. Clearly, there are many particles in the matrix which are below the resolution limit of the SEM. However, it is likely that not all of these particles are silicon carbide because it is known that aluminum carbide and aluminum oxide also exist in the matrix of this alloy even in the absence of silicon carbide (1).

An analysis of particle size distribution was made using a Dapple image analysis system. Both SEM and TEM photographs were used to obtain the distribution of particles shown in Fig. 5. Particles range in size over nearly three decades, and the distribution appears to be bimodal,
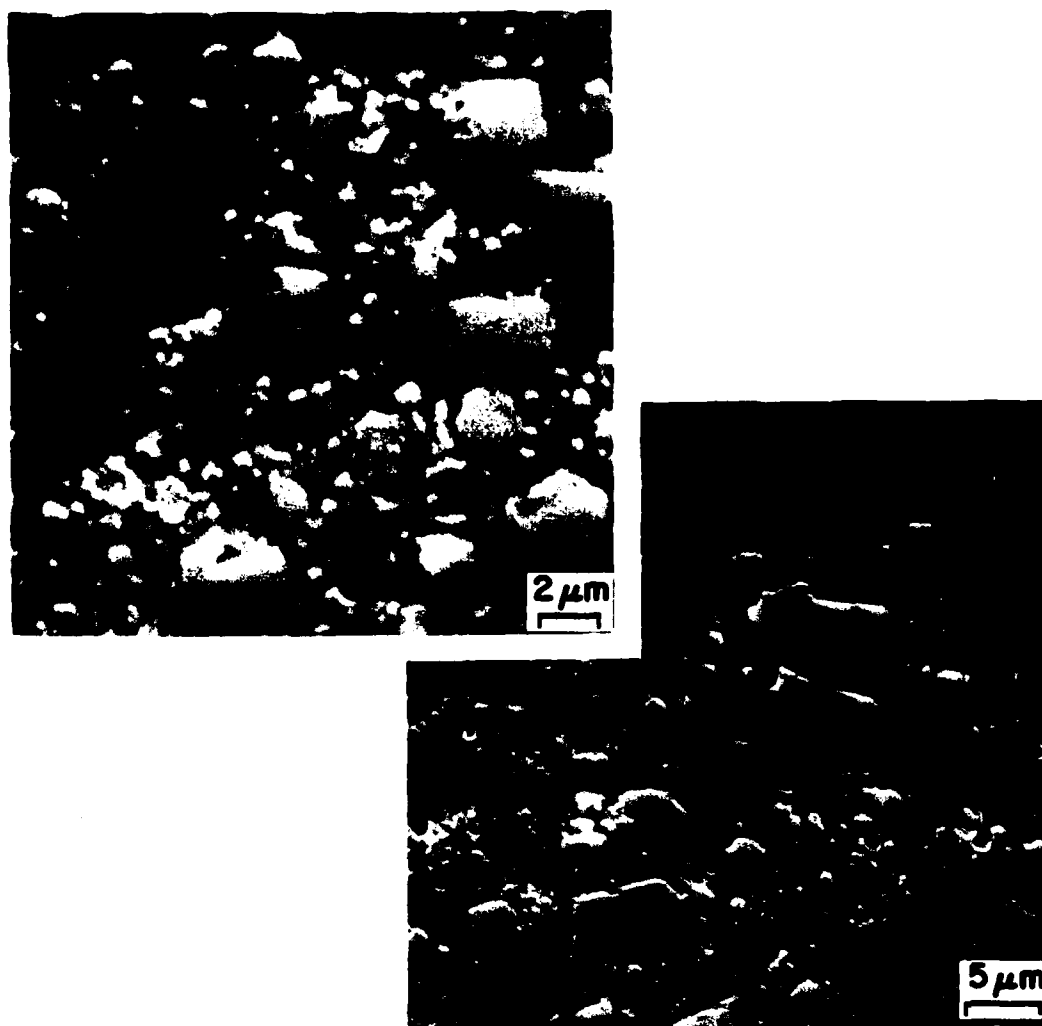
Figure 3. SEM of particle size and distribution. Material
has some agglomeration of particles and some voids.
The distribution of particles is reasonably uniform,
but there is a large range of particle sizes.
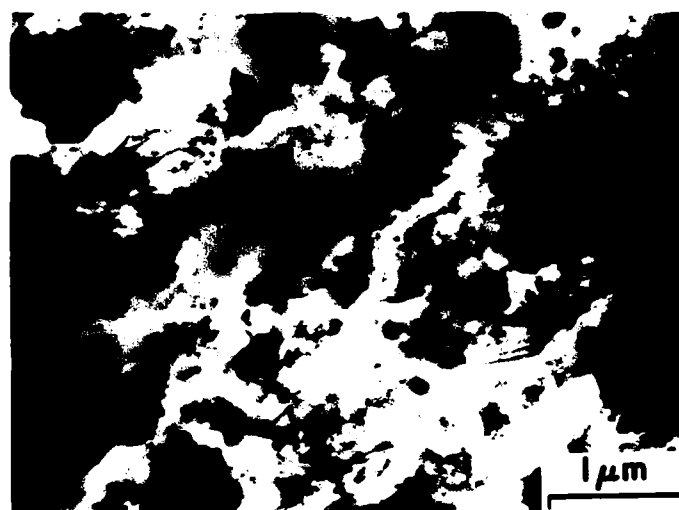
(a)
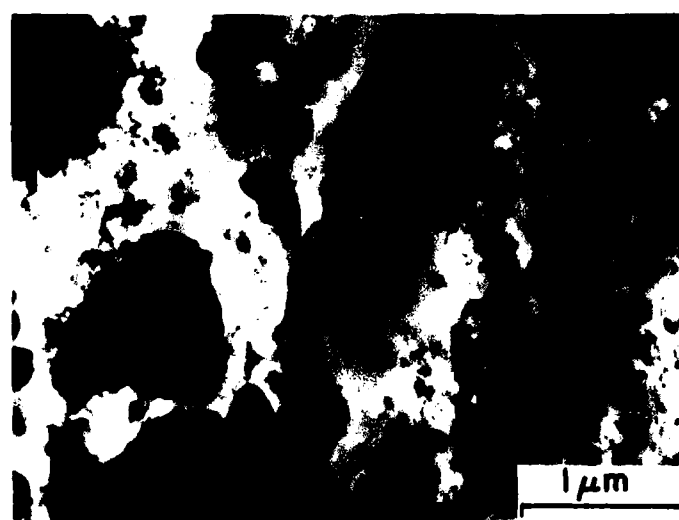
(b)

Figure 4. Transmission electron microscopy showing subgrains,
small particles and dislocations in the matrix.
Subgrains may be seen because of Moire fringes.
Particles are completely opaque to the beam while
the dislocation "clouds" are not. Note the lack
of dislocation clusters near particle-matrix in-
terfaces.
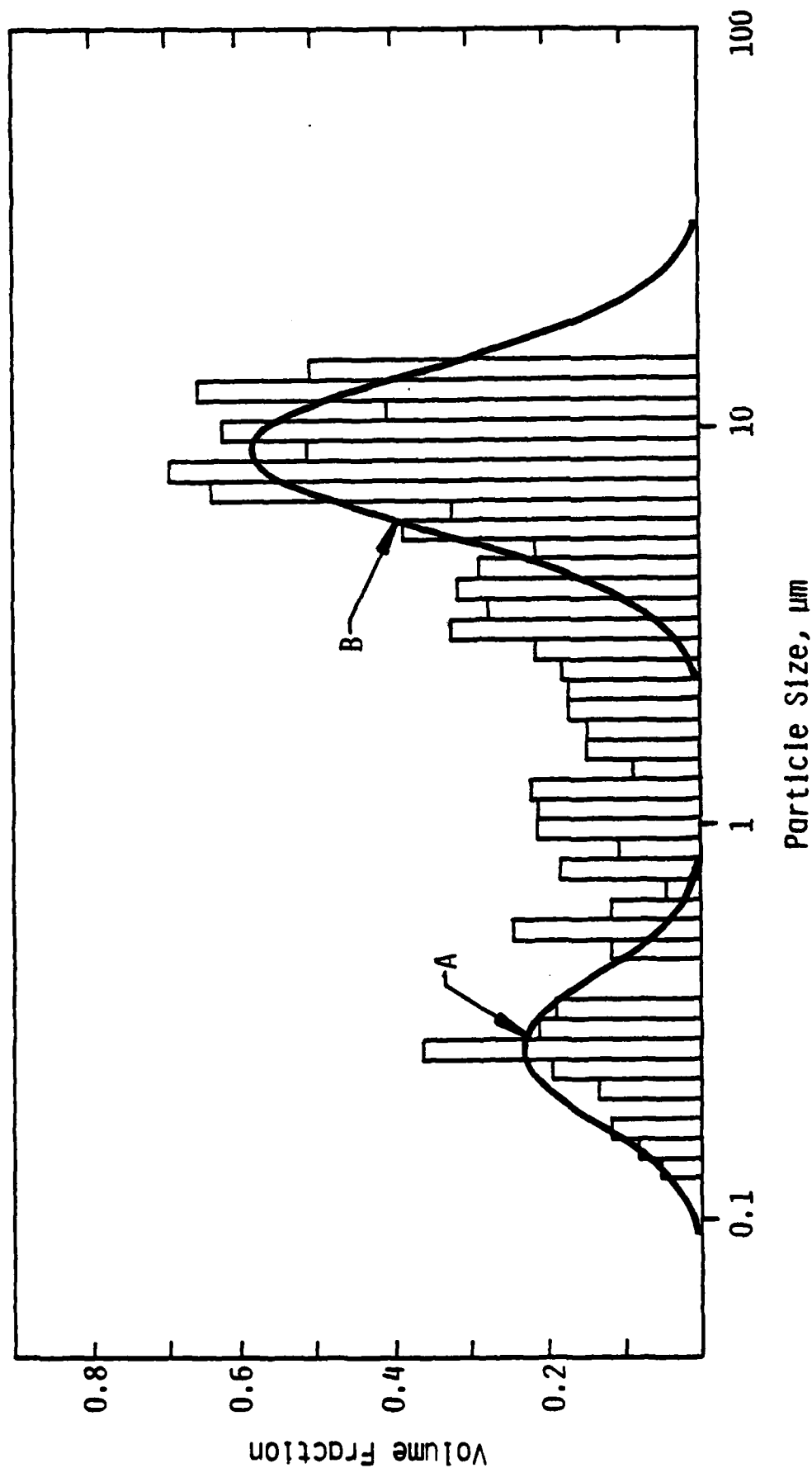
Figure 5. Volume fraction of particulate material in composite by size. All of the particles above about 1 μm are probably SiC, whereas many of the smaller particles, Curve A, are probably Al_4C_3, Al_2O_3 and MgO (1). See Table 2 for details of Curves A and B, which are log-normal fits to the data.

11

with one peak centered at about 0.3 µm and the other peak at approximately 9 µm. Almost 1200 particles were measured in the analysis, yet there is still uncertainty in the data. The lines shown in the figure assume a log-normal (Poisson) distribution and have been fit so that the unfilled area above and below the lines are about equal.

Volume fraction of particles is directly proportional to the area fraction measured by image analysis; thus, an estimate of volume fraction may be made from the data of Fig. 5. Measured total fraction of particles is 0.243. This is somewhat larger than the sum of the stated volume fraction of oxides and aluminum carbides in the base metal of 0.038 (1) and the volume fraction of 0.15 of added SiC particles. If Curve B of Fig. 5 is used to extrapolate the upper size range of particles, then volume fraction is increased to approximately 0.29.

A log-normal distribution function has been fit to the data to obtain Curves A and B. Derived values for the curves are shown in Table 2. Beneath Curve A, the volume of particles is 0.034, which compares well with the fraction (0.038) of oxides and carbides in the base metal (1). Although Curve B fits the large particle data reasonably well, it does not adequately represent the remaining particle size distribution. Volume fraction might also be considered to be approximately constant for particles ranging from about 0.7 µm to 5 µm, but above this size, there is clearly an increase in volume fraction.

2. **Subgrain Size:**

TEM micrographs also showed the existence of reasonably well formed subgrains. Measurement of subgrain size from 6 micrographs indicated a range in subgrain size of 0.4 to 0.9 µm, with an average of 0.67 µm. Misorientation of the subgrains was not measured, but from tilting foils

TABLE 2

IN-9052 + 15 v/o SiC
Data Summary

Subgrain size: 0.4-0.9 μm   Ave. = 0.67 μm

Microvoid size: 65% = 0.18-0.25 μm
5% = 0.26-0.44 μm
30% = 0.45-0.55 μm

Particle Size Analysis:

Curve	Average Size (μm)	Size Range 1 Standard Deviation (μm)	Size Range 2 Standard Deviations (μm)	Volume Fraction Within 2 Standard Deviations
A	0.29	0.19-0.43	0.13-0.64	0.034
B	9.0	5.72-14.1	3.6-22.1	0.17

Crack Tip Deformation:

ΔK MN/m$^{3/2}$	Crack Tip Strain ε_0	Plastic Zone Size (μm)
5.9	0.13	29
7.8	0.255	52

Total volume fraction - all particles = 0.243.

Volume including an extrapolation of Curve B = 0.29.

within the TEM it appears that crystallographic differences between the subgrains were more than a few degrees. These subgrains essentially constitute the grain structure of this alloy, there being no similar structure apparent when the composite was either chemically or ion etched. Many of the subgrains were somewhat elongated, having an aspect ratio of roughly 1.5-3:1, although some were nearly equiaxed.

3. **Surface Analysis:**

Spectra were obtained from specimens fractured within the vacuum system of an Auger electron spectrometer. The ratio of silicon to carbon was measured both in regions of matrix and on a few broken SiC particles found on the fracture surface. The particles showed a ratio Si/C of 46/54, which is stoichiometrically correct, while in the matrix, the Si/C ratio measured 25/75, indicating that excess carbon was present, as was expected from previous reports on composition of this alloy (1). The ratio Mg/Al was also examined in the matrix and was found to be somewhat variable, but averaging 0.05/95 ± 1, which was about as expected.

Ion milling of the fracture surfaces did not alter the Si/C ratio, nor did it uncover any particles previously hidden by a thin layer of matrix material, as has been reported for other aluminum alloy/SiC composites (2).

FRACTURE PATH

1. **Fatigue Crack Growth Sequence:**

The path of the crack through the composite was observed by cyclically loading specimens within the SEM. A typical representation of this is shown in Fig. 6, where it may be seen that the crack path was often
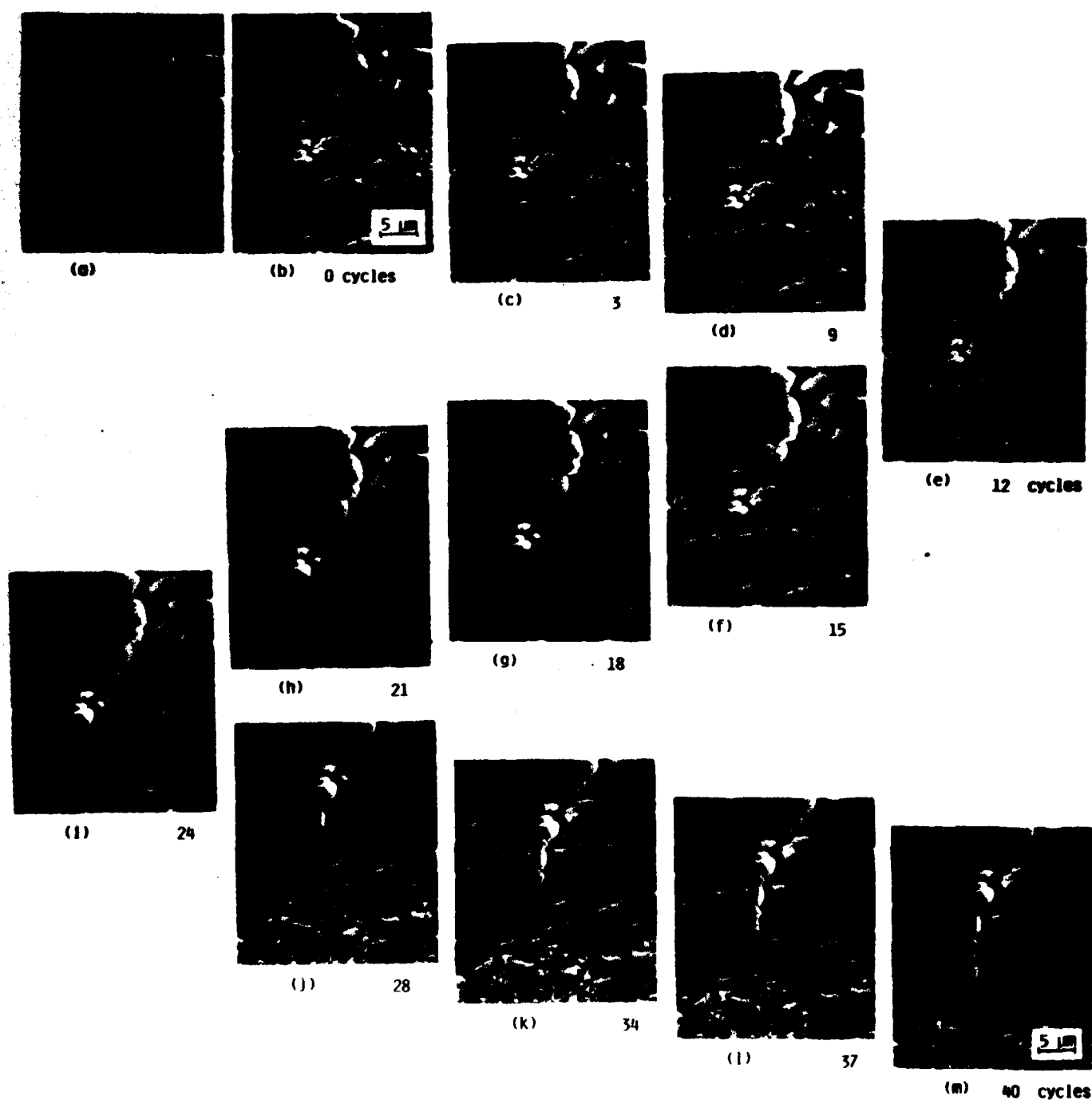
Figure 6. Fatigue crack growing through composite. In (a), the unloaded crack is tightly closed. Subsequent cycling (b-f) the crack moves around the SiC particles in its path, breaking into a small cluster of particles without matrix in between them at (g). At this point, a crack appears in the large rectangular particle just ahead of the crack tip. Subsequent cycling causes the crack path to go through that SiC particle (i) as it continues growing.

through regions of the matrix having an absence of visible particles, but that on occasion the crack path went through larger SiC particles and along the interface between particle and matrix. It should also be noted from the figure that crack growth rate is quite irregular. Sometimes the crack grows several micrometers in a few cycles, while at other times, several cycles are required before crack advance. This behavior is somewhat different than has been found for other unreinforced aluminum alloys (3,4), in that advances of several micrometers in a few cycles have not been seen previously.

2.   Fractography of Fatigue:

Fracture surfaces produced by cyclic loading were examined by both SEM and two-stage replicas viewed in the TEM. Stereopair photographs were made from matching locations of both fracture surfaces to verify that voids were not formed during fatigue crack growth. A matching set of photographs from both surfaces is shown in Fig. 7, together with a high resolution (replica) photograph which shows a few periodic markings. Out of dozens of replica photographs, these were the only such markings found. It is likely that these markings are striations. Spacing of these striations is about 0.055 μm, which from Fig. 1 corresponds to $\Delta K = 6.2$ MN/m$^{3/2}$, if one striation per cycle is assumed.

3.   Fractography of Rapid Fracture:

As may be seen in Fig. 8, the fracture surface caused by rapid crack growth is both similar and different relative to the fatigue fracture surface. The similarity is in the roughness of the surface, when viewed in the SEM, but the difference is in the formation of very small dimples which covered a large proportion of the fracture surface, as seen best in
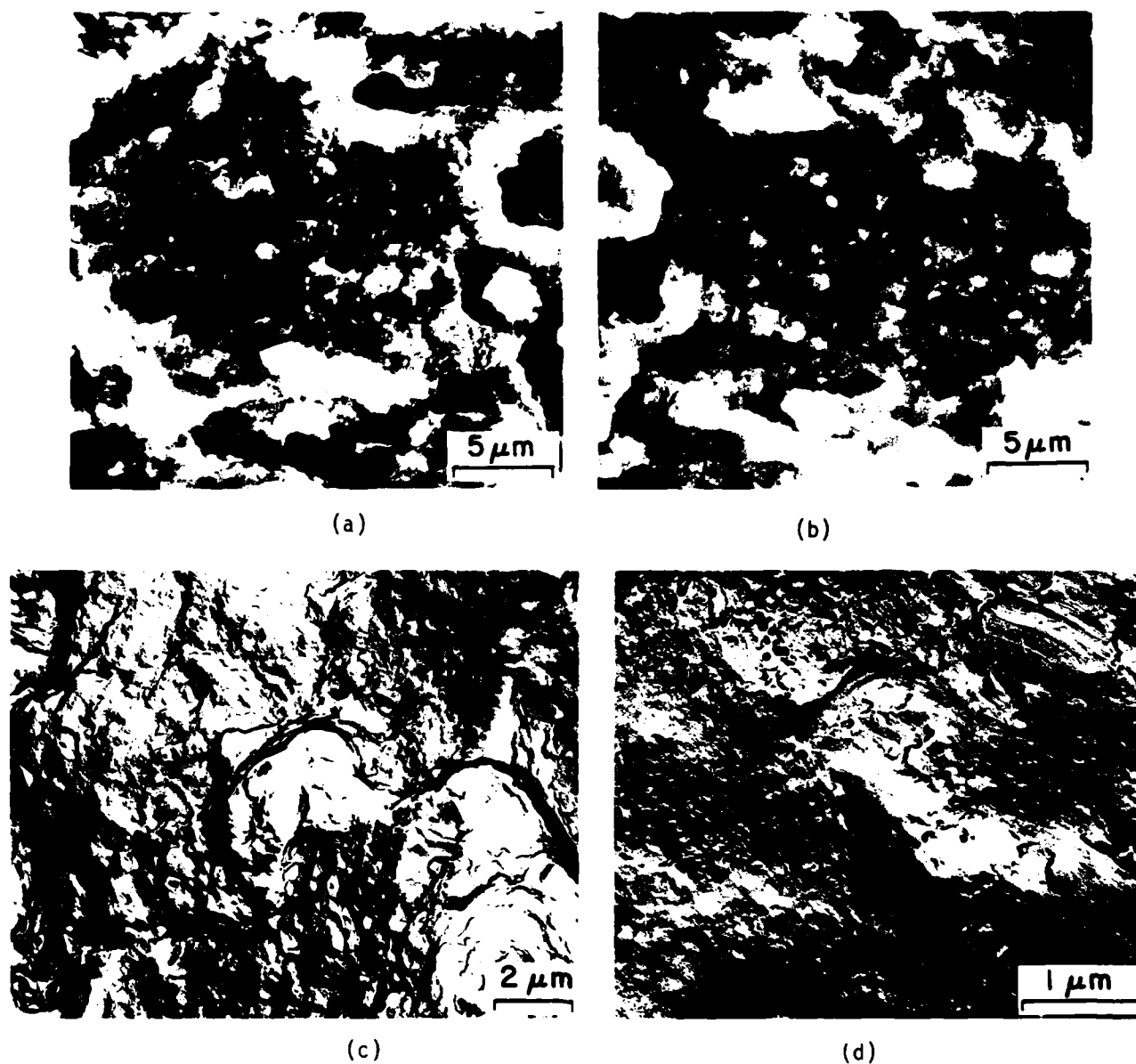
Figure 7. Fractography of fatigue. (a) and (b) are matching SEM micrographs of opposing surfaces at $\Delta K \simeq 7$ MN/m$^{3/2}$ showing rough topography, but no evidence of void formation. (c) and (d) are replica—TEM micrographs showing (c) relatively smooth (burnished) surface, and (d) a few extremely small striations.

(a)

(b)

(c)

(d)
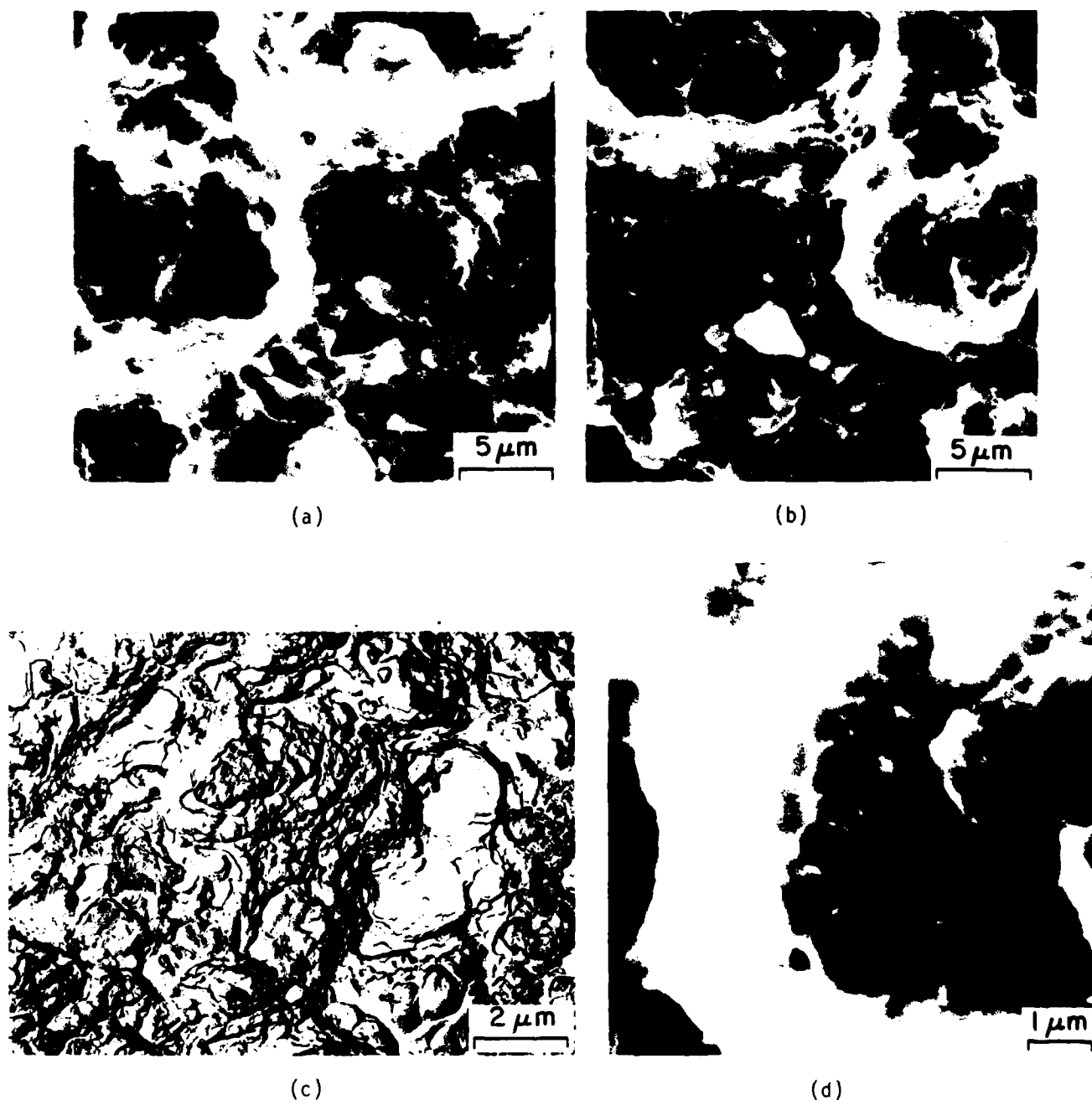
Figure 8. Fractography of rapid fracture. (a) and (b) are matching SEM micrographs of opposing surfaces having similar rough topography to the fatigue fracture, but which show evidence of very small dimples (voids). Also, note the fractured SiC particles. (c) is a replica—TEM micrograph which shows that a significant part of the surface is covered by equiaxed dimples, and (d) is a SEM micrograph [a close-up of (b)] showing how shallow these dimples are relative to their diameter.

the high resolution SEM and the replica photographs. The size of 140 well formed dimples found on replica TEM micrographs were measured: 65% had a size range of 0.18-0.25 μm, 5% a size range of 0.26-0.44 μm, and the other 30% measured 0.45-0.55 μm.

Based on fractography, it is apparent that the matrix-silicon carbide interfacial strength exceeds the ultimate strength of this composite. Only during fatigue was a crack found to be growing in an interface, Fig. 6. In the rapid fracture region, no debonding was observed. This strong interfacial region is shown in Fig. 9(a). Cracking of large SiC particles during rapid fracture was probably assisted by cracks already present in the particles. These cracks were formed some time during the manufacture of either particles or composite. An example of a cracked particle in as-received material is shown in Fig. 9(b). To reveal cracks like this, it was necessary to ion etch the surface, thereby relieving the compressive residual stresses in the matrix which were holding the cracks closed and rendering them invisible. Compressive residual stresses have been found in similar composites and quantified by Arsenault and Fisher (2).

Occasionally, broken SiC particles were found on the surfaces formed by fast fracture. The sizes of 37 broken particles found on fractographs were measured. The dimensions of these particles ranged between 2 and 11 μm, and averaged 5.5 μm, which is slightly smaller than the average size of the particles within the large-particle size distribution, Fig. 5, Curve B.

(a)
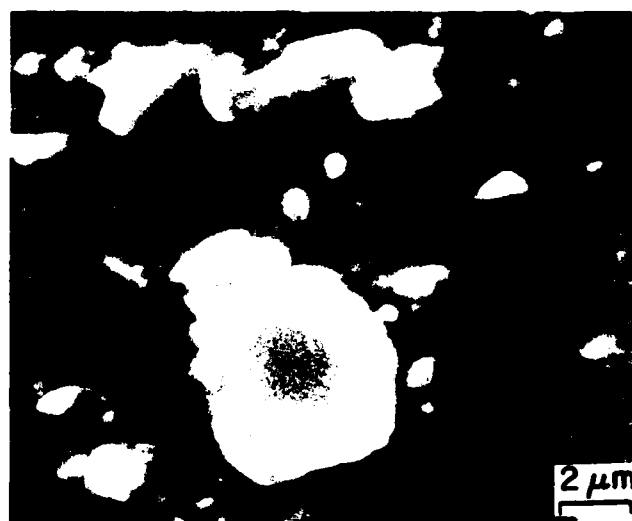
(b)

Figure 9. Fracture of silicon carbide particles. A few broken SiC particles having diameters $2 < d < 11$ μm were found on overload fracture surfaces. (a) Interface between broken particle and matrix showing a lack of separation, indicative of a strong bond. (b) Cracks in SiC particles existed prior to loading but they were held tightly closed. The crack revealed here was opened by ion milling away the matrix, which relieved residual stresses holding the crack closed.

CRACK TIP STRAINS

Typical distributions of shear strain in the near crack tip region are shown in Figs. 10 and 11 for fatigue cracks. In Fig. 10, strain is plotted along the vertical axis and a "net" is used to cover all the points, thereby displaying strain within the entire crack tip region. The crack is shown schematically on the plane of zero strain. Conversely, Fig. 11 shows a contour plot of strain around the crack tip, which is much harder to understand, but this latter representation has the advantage of registry with the photograph, so that strain may be correlated with particle location. Examination of this and other similar photographs indicated that, in fact, there was no simple correlation between strain magnitude and particle location. It is even less clear, considering this result, just why the Voight averaging method of computation, which assumes equal strain in particle and matrix, gives an unusually high value of modulus.

A typical distribution of strain parallel to the loading axis is shown in Fig. 12. These data may be represented by the function

$$\epsilon(x) = \epsilon_0 (x + x_0)^{-p} \qquad (4)$$

From Fig. 12, and 15 other similar analyses, it is evident that $p = 1.1$ and $x_0 = 1$ um fit most of the data well, leaving only ϵ_0 to be determined as a function of stress intensity factor. An average value of $\epsilon_0 = 0.13$ was measured at $\Delta K = 5.9$ MN/m$^{3/2}$, while at $\Delta K = 7.8$ MN/m$^{3/2}$, average $\epsilon_0 = 0.255$. Plastic zone size was determined by extrapolating Eq. (4) to a limiting strain value. When the elastic strain (σ_y/E) is used, the average crack tip - plastic boundary distances obtained were 29 um at $\Delta K = 5.9$
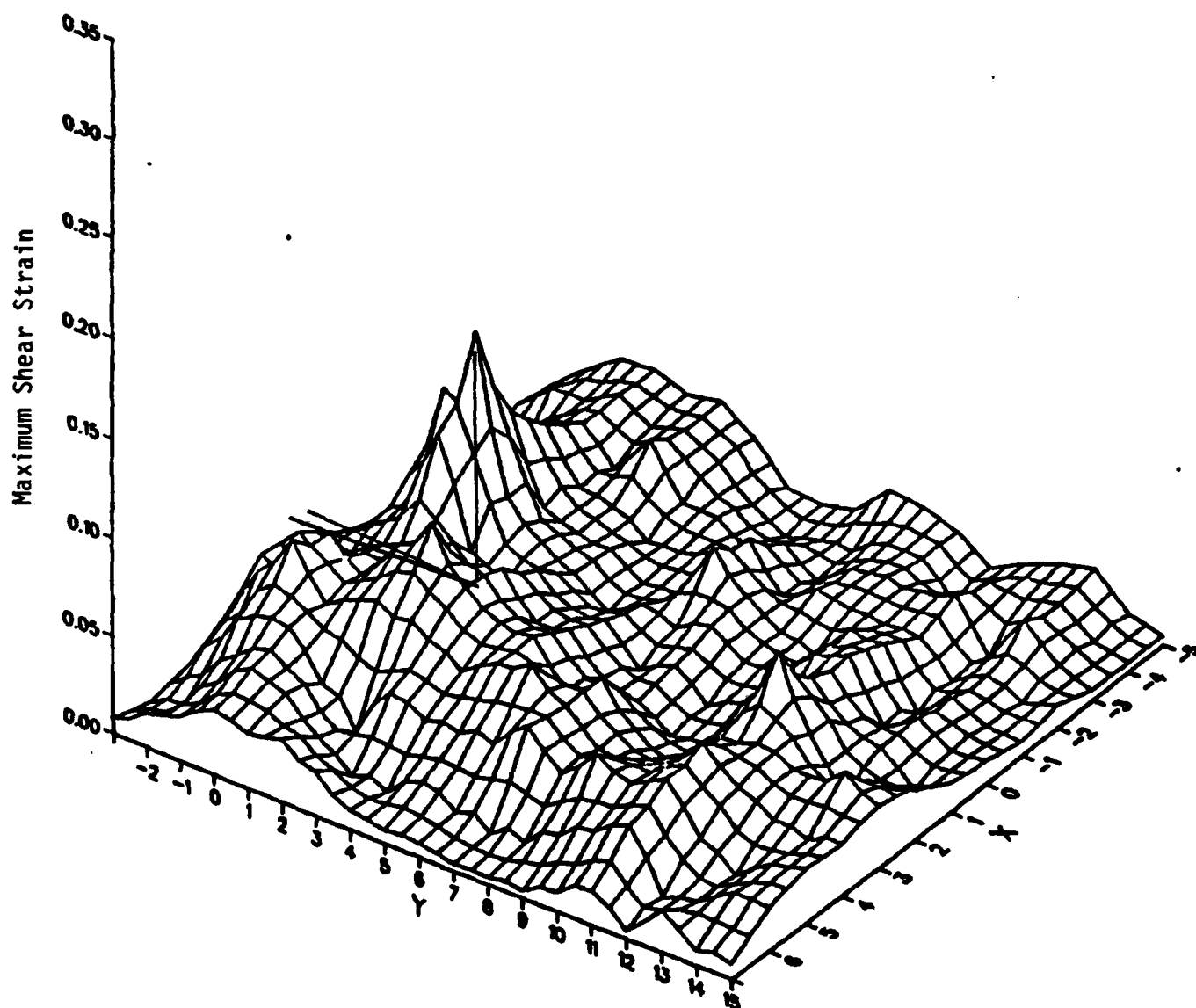
Figure 10.   Distribution of maximum strain around crack tip showing
the inhomogenous nature of the strain field.   Crack is
schematically shown on the plane of zero strain.   X
and Y are in micrometers.   This strain distribution
corresponds to the near crack tip portion of Figure 6(i).
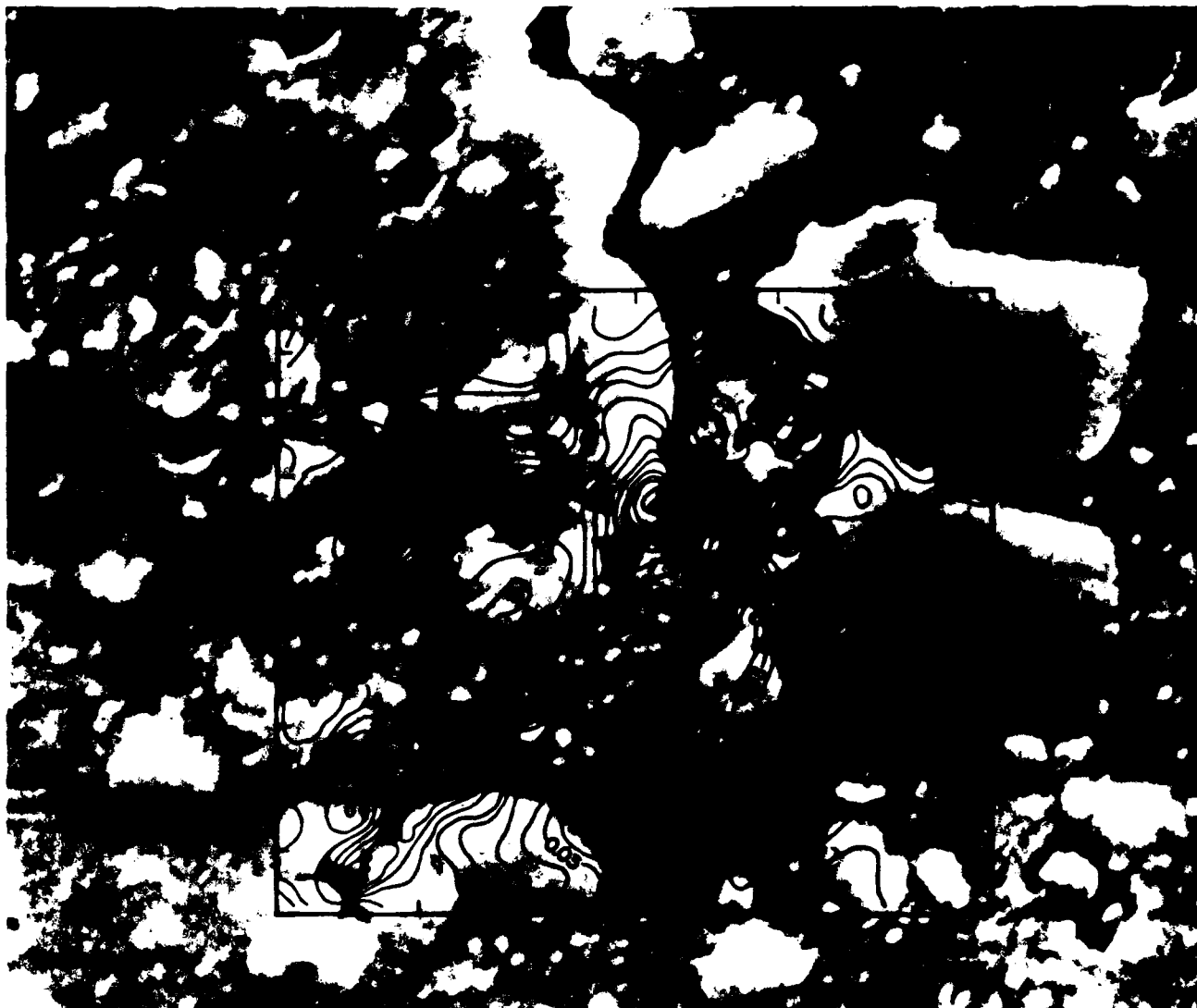
Figure 11.   Contours of maximum shear strain superimposed on a crack tip
             region. Magnitude of strain is apparently independent of
             SiC particle location. Subsequent crack growth was along
             the region of maximum strain extending down to the left
             from the tip.

Figure 12. Example of strain distribution parallel to loading axis.
x is the distance from the crack tip.

$MN/m^{3/2}$ and 52 µm at $\Delta K = 7.8$ $MN/m^{3/2}$. These same values may be computed from $\alpha(K/\sigma_y)^2$, where $\alpha = 0.045$.

Crack tip opening displacement (CTOD) has previously been found to be related to crack tip strain for a number of aluminum alloys (3,4)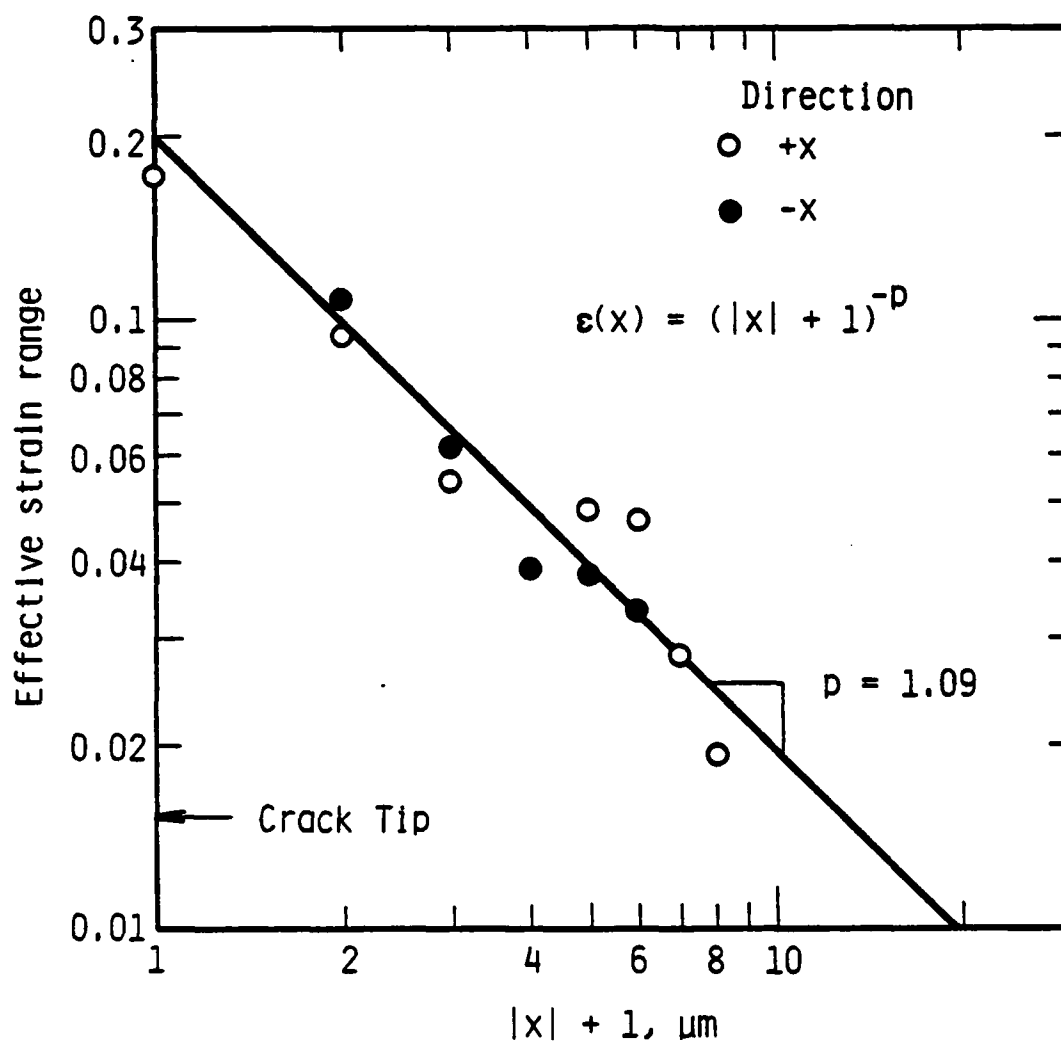. This correlation for the present composite and its unreinforced matrix alloy is shown in Fig. 13. There is a clear difference between the unreinforced matrix and composite, which indicates that the crack tip profile changes differently in the two materials as ΔK is increased.

COMPUTATION OF FRACTURE TOUGHNESS

Fracture toughness, K_{Ic}, of any material is proportional to the work done per unit area of new surface created, G_e, by the material as it is torn apart. The relation between them is

$$G_e E = K_{Ic}^2 \tag{5}$$

There are three components which contribute to G_e in a ductile material: (1) the work done within the plastic zone surrounding the crack tip as the crack passes through, (2) the work done in formation of the void sheet on the fracture surface, and (3) the energy required in creating new fracture surface. Thus, the work done during fracture becomes

$$G_e = dWp/dA + dWv/dA + SE \tag{6}$$

where the first term is the work per unit area of crack done by plastic flow, the second is due to void sheet formation, and the last is the surface energy term. The magnitudes of these contributions to G_e are
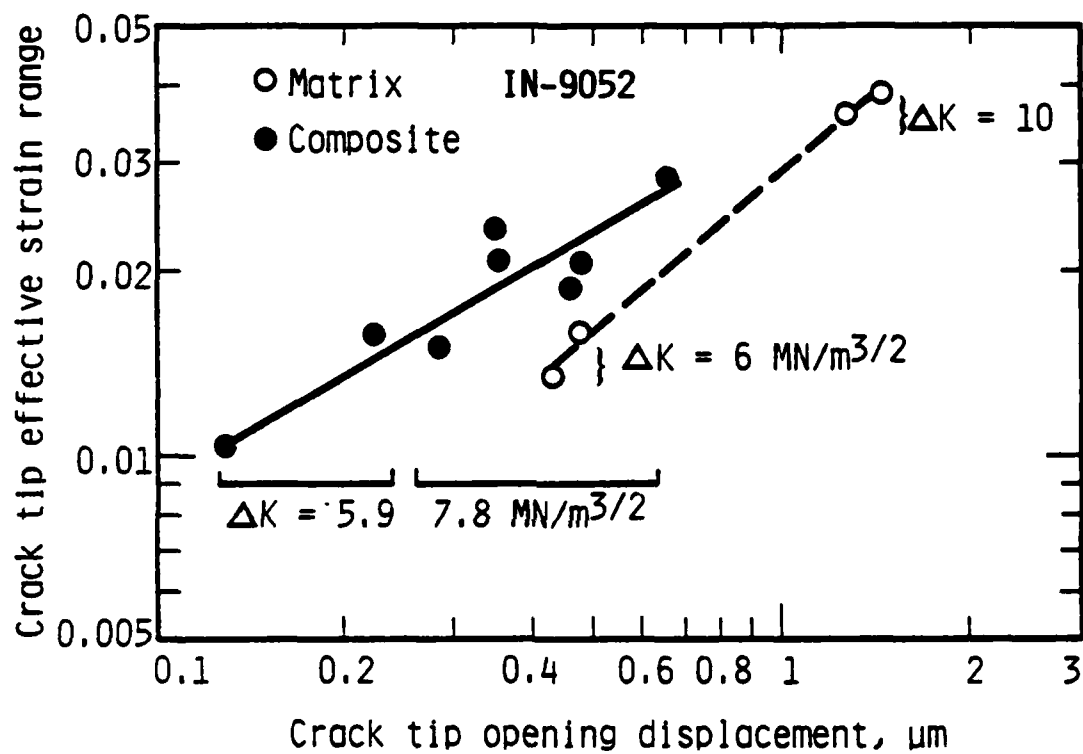
Figure 13.   Correlation between crack tip effective strain and CTOD
for SiC reinforced and unreinforced IN-9052.

expected to decrease in the order of listing. The work done by plasticity and void sheet formation has been computed as follows.

1. Plastic Zone Work:

The work done within the plastic zone of the crack has been computed from the stress strain curve and strain distribution perpendicular to the direction of crack growth. Appendix 1 describes how the computation was performed, and it should be noted that the unloading part of the stress-strain curve is important, and has been included. The value computed for work dissipated within the plastic zone per unit area of new crack, using the measurements of strain made at the ΔK just below unstable crack growth, is $7.6 \pm 1 \times 10^{-4}$ MJ/m^2. This value is then used in the relation

$$(dWp/dA) \ E = K_p^2 \tag{7}$$

to compute the fracture toughness component attributed to the plastic zone. The value of K_p thus computed is $7.95 \pm .05$ MN/m$^{3/2}$.

2. Void Sheet Work:

The work expended in creating the void sheet, dWv/dA, has been computed with the model given in Appendix 2. Using values of void size and plausible estimates of void shape and surface coverage, the value of dWv/dA was found to be about $9 \pm 3 \times 10^{-5}$ MJ/m^2, or approximately a factor of ten less than the work expended within the plastic zone. By adding this work to that dissipated within the plastic zone, the fracture toughness computed (Eq. 7) is increased to 8.5 MN/m$^{3/2}$, which is approximately equal to the value measured.

3. Fracture Surface Work:

The surface energy of aluminum has a value of approximately 2×10^{-6} MJ/m^2.

DISCUSSION

1. Tensile Properties:

The stress strain curve of this composite shows less of a distinctive yield behavior than is normally exhibited by unreinforced aluminum alloys. The shape is distinctly parabolic, and the value of yield approximately coincides with the proportional limit, as measured by periodic unloading. The stress at a strain of 0.2% offset is roughly twice the proportional limit, which is closer to the value of yield stress normally listed for aluminum alloys, but if this value is used for yield, then modulus would be much lower than has been measured from the unloading curves. Computed value of modulus (Reuss approximation) is nearly that measured. Clearly, this alloy has an unusually high work hardening coefficient ($n = 0.6$).

Yield stress may be computed for a particulate strengthened material using the analysis attributed to Orowan by Martin (5). First, the yield strain is computed from the following relation

$$\gamma_y = \frac{.81b}{2\pi(1-\nu)^{.5}} \frac{\ln(\frac{2r_s}{b})}{\lambda_s - 2r_s} \tag{8}$$

where $2r_s$ = particle size, λ_s = the mean particle separation distance, b = Burgers vector, and ν = Poisson's ratio. Yield stress is then

$$\sigma_y = 2G\gamma_y \qquad\qquad (9)$$

Using these equations, yield stress of the composite may be computed from the volume fraction and particle size data in Fig. 5. A broad range of particle sizes cannot be handled directly by the equations, so it is necessary to approximate the particle size distribution by adding together the effects of several peaks. To the two peaks given in Table 2, an additional peak centered at 0.9 μm, having a volume fraction of 0.055 is assumed, in order to account for particles between Curves A and B. Curve A was adjusted to be centered at 0.2 μm, with a volume fraction of 0.055, which is not unreasonable. Using these three particle size peaks to calculate stress and then adding together the contribution of each gives a value of yield stress = 250 MPa, which is acceptably close to the 280 MPa value measured. No account is taken by this analysis of the very small subgrain size of the matrix which undoubtedly contributes to the yield stress. In the base alloy, a high dislocation density also adds to the yield stress, but the micrographs of Fig. 4 indicate a lower initial density for this composite than was evidenced in the base alloy (1), so the expected contribution of this factor would be small.

2. **Fracture Properties:**

   a. **Subcritical Crack Growth:**

   Fatigue crack growth rate, as described by Eq. (1), has a larger value of exponent s and a higher ΔK_{th} than the unreinforced alloy, although it should be emphasized that this threshold was derived from crack growth rates of 10^{-7} to 10^{-9} m/cy. This behavior is, in general, in

agreement with that reported by Liaw (6) for a series of SiC fiber rein-forced aluminum alloys. Larger crack growth rates than the matrix alloy are not surprising considering the results of Fig. 13. Apparently, the damage done on each loading cycle in the composite is greater than in the unreinforced alloy; more strain (damage) can be supported by a given CTOD in the alloy than in the composite. This behavior is further demonstrated by the sequential photographs of Fig. 6.

b. Rapid Fracture:

Fracture toughness of the composite is much lower than that of the unreinforced alloy (8.9 vs 29 $MN/m^{3/2}$). The reasons for this are three fold: (1) the crack tip is not sustaining large strains, (2) the plastic zone attending the crack is small, and (3) voids formed during fracture are very small. If the theory of Brown and Embury is considered to be directly applicable, then the reason for the small crack tip strain is the small interparticle spacing of this composite, which is a function of both particle size and the volume fraction. But, since that theory is very simplistic and of questionable applicability, there are probably other factors controlling this behavior.

The size of the plastic zone surrounding the crack is much smaller than the dimension estimated using fracture mechanics; the K^2 de-pendency is sustained, but the proportional factor (a) is about one-fourth that derived by analysis. Strain decreases with distance from the crack tip as $r^{-1.1}$ rather than the $r^{-.5}$ predicted analytically, which limits the plastic zone size. Clearly, more work would be done during fracture if the plastic zone size were larger, since the work done in the plastic zone (Appendix 1) is a fairly sensitive function of the plastic zone size. The

factors controlling plastic zone size are strain at the crack tip, stress distribution around the crack tip, and (perhaps) the work hardening characteristics of the material. The approximate correlation of void size with subgrain size is consistent with the findings of Wilsdorf, et al (7), who found, using high voltage TEM, that microvoids were initiated at subgrain boundaries. Microvoids have been found to form at particle-matrix interfaces, but fractography, Fig. 8, has shown the lack of particles related to dimples, and the particle-matrix interfacial strength has been found to be greater than the strength of the larger SiC particles, Fig. 9(a). The model of work done in void formation, Appendix 2, indicates that more work would be expended in fracture if the voids were larger, thereby increasing the strain associated with void formation. Of course, the possibility also exists that a larger strain is not sustainable in the matrix due to the particle volume fraction and size distribution.

Crowe, Gray and Hasson (8) computed fracture toughness from the dimensions of fracture surface dimples. They measured dimple size and height from the fracture surfaces of particulate SiC in 6061 made by powder metallurgy and found dimple diameters of 3.7-3.9 μm, with heights of 1.2-1.4 μm, giving height/diameter $(^h/d) \cong .34$. Using this ratio with the void diameters measured for IN-9052/SiC (average size $\cong$ .3 μm, from Table 2) allows computation of K_{IC} = 2.5 MN/m$^{3/2}$, which is much lower than that measured. Or, making the computation in reverse order for K_{IC} = 8 MN/m$^{3/2}$ gives $^h/d \gtrsim 1$, which is much larger than found.

These authors (8) also used a computation of fracture toughness attributed to Bates which consists of using dimple size and particle size to compute a value of critical CTOD at fracture. Using this computational

method for the present alloy results in $K_{Ic} \cong 0.31$ MN/m$^{3/2}$ which is approximately the value determined by the model of Appendix 2. Fracture toughness may also be computed from measured values of crack tip opening displacement using the concepts developed by Rice and Johnson (9), in which K_{Ic} is related to CTOD by

$$K_{Ic} = (2E\sigma_y \ CTOD)^{.5} \tag{10}$$

Using the largest value of CTOD for the composite from Fig. 13 gives a value of $K_{Ic} = 5.7$ MN/m$^{3/2}$, which is considerably below the value measured. These computations reinforce our model results which show that the principal work to fracture for this composite is by deformation within the plastic zone rather than by formation of the void sheet.

It is possible that work to fracture expended in forming the void sheet could be increased by two means: size of the subgrains could be increased, thereby increasing void size, which would cause the strain to fracture, therefore the work, to be increased. The strength of the matrix-particle interface could also be decreased, which would cause voids to initiate at the SiC particles rather than at subgrain boundaries. This probably would result in an increase in the void size, thereby leading to an increase in both fracture strain and work done in formation of the void sheet.

c. **Interfacial Strength:**

An estimate of interfacial strength may be made using the analysis of Argon, Im and Safoglu (10). The ratio of radial stress component σrr/yield stress may be computed using the following equation:

$$\sigma_{rr}/\sigma_y = C_2 + (1+C_1)(\gamma/\gamma_y)^{1/n} \qquad (11)$$

where C_1 and C_2 are numerical constants computed from particle size and volume fraction (10). Interfacial stress is dependent on strain in the matrix, as would be expected. Performing this calculation gives a stress in the interface of about 600 MPa at yield strain, and over 3000 MPa at tensile fracture strain. These stresses may be compared with those estimated to have been required to break SiC particles found on the fracture surfaces. Because of the small size of these particles (2 to 11 μm) the size of flaws within the particles (a) cannot have exceeded 0.5-5 μm. The fracture toughness of SiC (as measured on bulk single crystals) is approximately 4 MN/m$^{3/2}$, and using the relation $K = \sigma\sqrt{\pi a}$, , the stresses required to fracture these small particles are within the range 1000-3000 MPa, which agrees very well with the stresses computed using Eq. (12). Flom and Arsenault (11) estimated a value of 1650 MPa using entirely different methods.

All these estimates of interfacial strength are reasonably consistent and indicative of an excellent bond between SiC and matrix.

SUMMARY AND CONCLUSIONS

Fracture toughness and fatigue crack growth in this mechanically alloyed composite have been investigated by a variety of techniques. The contributions to fracture toughness from plastic zone and void sheet formation were modeled, and a computed value of K_{IC} was compared to that measured. Modulus and yield strength were both measured and computed.

1. Yield strength may be computed from a knowledge of particle size and volume fraction. Modulus may be computed using the Reuss method of combining the moduli of particle and matrix.

2. Work expended within the plastic zone accounts for most of the toughness measured. Formation of the void sheet accounts for a much smaller part of the toughness than the plastic zone.

3. Larger silicon carbide particles break during fast fracture and occasionally during subcritical crack growth. Particle-matrix interface fracture is very rare, and only observed during fatigue crack growth. Estimates of interfacial strength exceed 1000 MPa, and may be as high as 3000 MPa.

4. Void nucleation is apparently from subgrain boundaries, rather than from particles, because of the high particle-matrix interfacial strength.

ACKNOWLEDGEMENT

REFERENCES

1.   S. K. Kang, D. L. Erich and H. F. Merrick, "High-Strength Powder Metallurgy Aluminum Alloys", M. J. Koczak and G. J. Hildeman, eds., pp. 317-328, TMS-AIME, Warrendale, PA, 1982.

2.   R. J. Arsenault and R. M. Fisher, Scripta Met., 1983, Vol. 17, pp. 67-69.

3.   D. L. Davidson and J. Lankford, Fatigue of Engg. Mat. and Struct., 1983, Vol. 6, pp. 241-256.

4.   D. L. Davidson and J. Lankford, Fatigue of Engg. Mat. and Struct., 1983, Vol. 7, pp. 29-39.

5. J. W. Martin, "Micromechanisms in Particle-Hardened Alloys", p. 62 and pp. 109-114, Cambridge Univ. Press, Cambridge, 1980.

6. W. A. Logsdon and P. K. Liaw, Engg. Frac. Mech., (accepted for publication), 1986.

7. R. N. Gardner, T. C. Pollock and H. G. F. Wilsdorf, Mat. Sci. and Engg., 1977, Vol. 29, pp. 169-174.

8. C. R. Crowe, R. A. Gray and D. F. Hasson, "Proceedings Fifth International Conference on Composite Materials ICCM-V", pp. 843-866, TMS-AIME, Warrenville, PA, 1985.

9. J. R. Rice and M. A. Johnson, "Inelastic Behavior of Solids", pp. 641-672, McGraw Hill, New York, N.Y., 1970.

10. A. S. Argon, J. Im and R. Safoglu, Met. Trans. A, 1975, Vol. 6A, pp. 825-837.

11. Y. Flom and R. J. Arsenault, Mat. Sci. and Engg., 1986, Vol. 77, pp. 191-197.

12. D. L. Erich and S. J. Donachie, "Benefits of Mechanically Alloyed Aluminum", Metals Progress, 1982, Vol. 121, pp. 22-25.

13. L. M. Kachanov, "Foundations of the Theory of Plasticity", p. 191, North Holland Publishing Company, London, 1971.

APPENDIX 1

As was shown in Fig. 2, the stress-strain curve for this material may be described by

$$\sigma = \sigma_y \frac{\epsilon}{\epsilon_y}^n \tag{1-1}$$

The work expended by straining an element of material an amount ϵ_t is

$$W = \int_0^{\epsilon_t} \sigma_y \left(\frac{\epsilon}{\epsilon_y}\right)^n d\epsilon = \frac{\sigma_y \epsilon_y}{n+1} \left(\frac{\epsilon_t}{\epsilon_y}\right)^{n+1} = W_0 \, \epsilon_t^m \tag{1-2}$$

If the element is near a moving crack, it unloads due to crack passage, and some elastic strain is recovered, resulting in somewhat less work being expended within the element. This results in the work to fracture of an element within the plastic zone of a passing crack being

$$W = W_0 \epsilon_t^m \left[1 - \frac{1}{2} \frac{W_0 m^2}{E} \epsilon_t^{(m-2)}\right] \tag{1-3}$$

where the term within brackets is that due to elastic recovery. This condition is depicted in Fig. 1-1(c).

To compute the work expended by material deformation within the plastic zone per length of extending crack, consider the condition depicted in Fig. 1-1, which shows in (a) the motion of the plastic zone as the crack moves from y_1 to y_3. All elements between y_2 and y_3 have experienced a strain history $0 \to \epsilon_t \to 0$, as shown in Fig. 1-1(b), dissipating the work W_A. In addition, the work W_B was expended as the crack moved from y_1 to y_3, but the work W_C had already been done, and in the steady
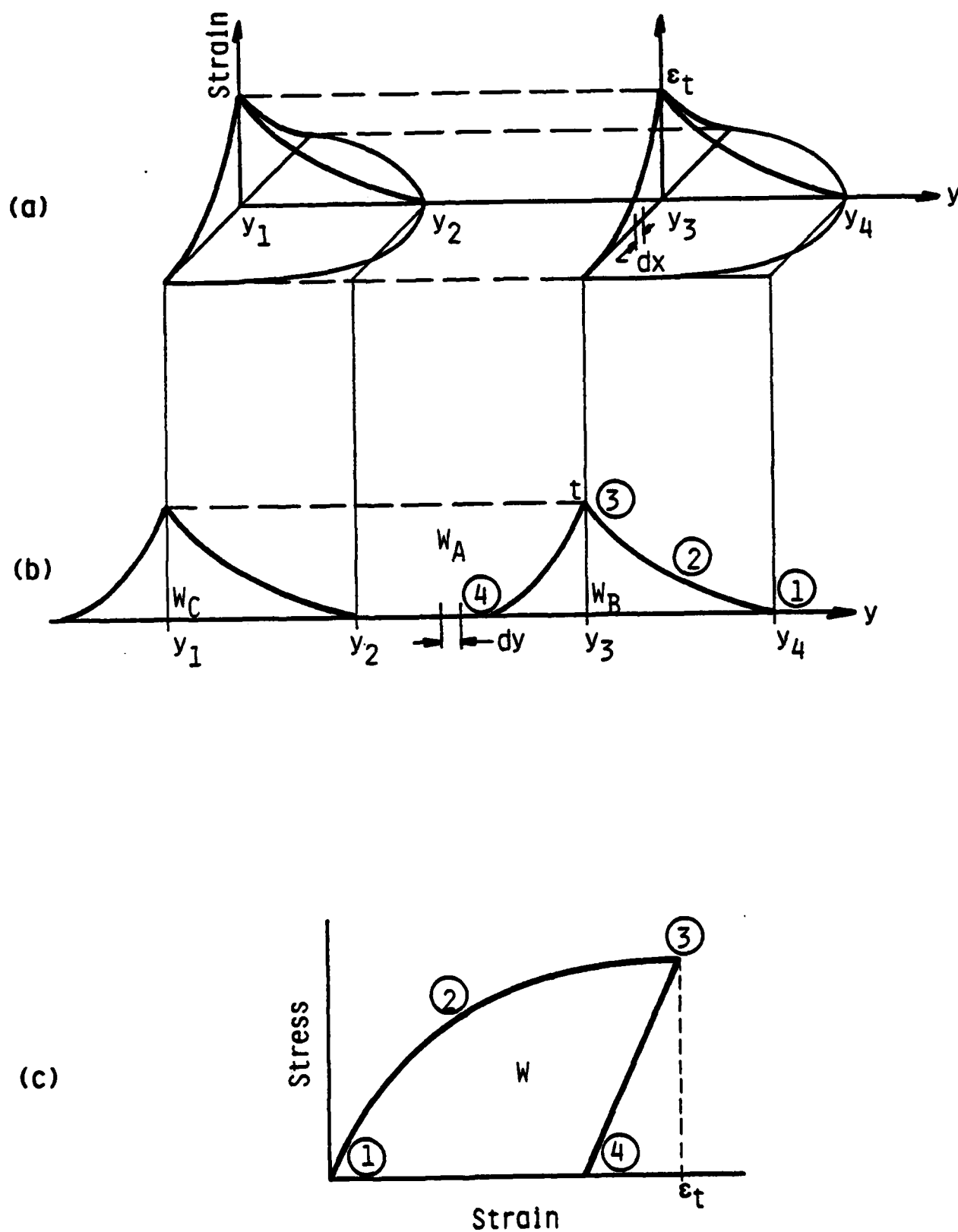
Figure 1-1. Movement of the crack tip plastic zone with crack growth along y, depicted schematically in (a) and (b), and (c) the relationship between the stress-strain curve and the plastic zone.

state $W_B = W_C$. Therefore, only the computation of W_A is necessary in order to obtain the work expended per unit length of unstable crack growth:

$$W_A = \int_0^x W(x)dx \qquad (1\text{-}4)$$

where $W(x)$ is given by Eq. (1-3). $\varepsilon(x)$ is the strain distribution within the plastic zone perpendicular to the direction of crack growth. From Eq. (4), $\varepsilon(x) = \varepsilon_0(x + x_0)^{-p}$; combining this with Eq. (1-3) gives

$$W(x) = W_0[\varepsilon_0(x + x_0)^{-p}]^m \{1 - \frac{W_0 m^2}{2E} [\varepsilon_0(x + x_0)^{-p}]^{m-1}\} \qquad (1\text{-}5)$$

This equation has been parameterized to

$$W(x) = C_1 (x + x_0)^{-\ell} - C_2(x + x_0)^{-r} \qquad (1\text{-}6)$$

Putting this in Eq. (1-4) and integrating gives

$$W_A = C_a (x_0 + x)^a + C_b(x_0 + x)^b \qquad (1\text{-}7)$$

where $\quad C_a = \dfrac{W_0 \varepsilon_0^m}{a}$, $C_b = \dfrac{W_0^2 m^2}{2Eb} \varepsilon_0^{2(m-1)}$, $a = 1-pm$, and $b = 1-2p(m-1)$.

From the stress-strain curve, the strain distribution perpendicular to the crack growth direction and the elastic modulus, the work expended per unit area during crack passage may be computed.

APPENDIX 2

THE WORK OF FORMING THE VOID SHEET

During rapid fracture, voids initiate and grow as the crack front passes. The work expended in forming the voids covering the fracture surface has been estimated using the following model.

To derive the work done in void formation, the area beneath the tensile stress-strain curve is again used, as in the computation of work done within the plastic zone. Therefore, the problem reduces to one of determining the maximum strain accompanying the formation of voids. No method of measuring this strain has been found; thus, the void formation strain has been estimated.

Voids seem to have initiated at subgrain boundaries; therefore, the initial size is zero. The final shape of the void is considered to be an ellipsoid of major axis a and minor axis b. A portion of fracture surface containing voids of this geometry is shown schematically in Fig. 2-1. The original and final lateral dimensions, l and w, remain unchanged during the formation of the voids. The height of the volume h absorbs all the volume increase V_I due to void formation.

Original volume = lwh; final volume = lwh + V_I; $V_I = \frac{4}{3} N\pi a$ (N = no. of voids).

Final height of the slab, h', then becomes
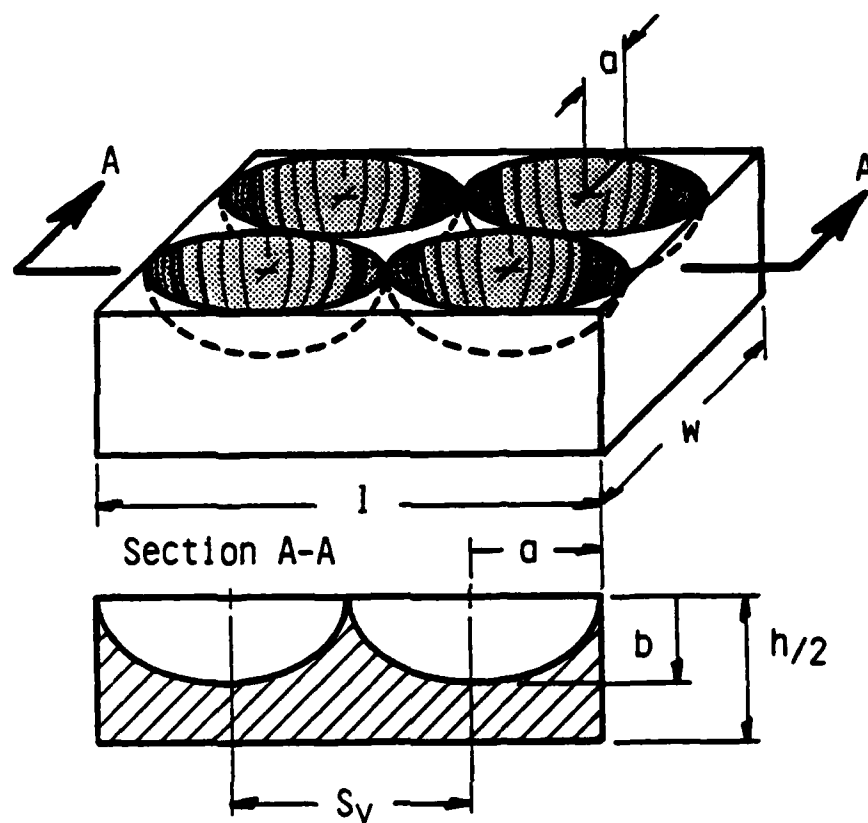
$$h' = \frac{lwh + V_I}{lw} = h + \frac{1}{3} \pi b$$

Figure 2-1. Geometry of void formation as modeled.

The work expended in deforming material to this strain is

$$W = W_o(\frac{\pi}{3}\frac{b}{h})^m \times \text{(unloading correction)}$$

The work per unit area of void sheet formation is

$$W_v = Wh = W_o(\frac{\pi}{3}b)^m h^{1-m} \times \text{(unloading correction)} \qquad (2-1)$$

Thus, the relationship between b and h determines the work done in fracture. Slip line theory (13) has been invoked to obtain estimates of h. Reasonable estimates of h range from being equal to void spacing S_v, which gives W_v a lower bound to being $S_v/3$, which gives W_v an upper bound.

From looking at stereopairs of replicas of the fracture surface, such as Fig. 8, a reasonable estimate of the void shape is $b = {}^a/5 = S_v/5$. This allows an estimate of strain of 0.2 to 0.6, which results estimates of work to form the void sheet of $1-2.2 \times 10^{-4}$ J/m^2. This assumes all microvoids have the size range summarized in Table 2 and that the surface is completely covered. From photographs such as Fig. 8, it is apparent that the entire fracture surface was not covered by dimples; an estimate has been made that only 60% of the fracture surface was covered with well formed dimples. Therefore, it is estimated that W_v

$$W_v = 6 - 13 \times 10^{-5} \text{ MJ/m}^2 \qquad (2-2)$$

The remainder of the fast fracture surface is covered by more smooth features, which are indicative of even less plasticity, thereby requiring even less work to form during passage of the crack front.

END

DTIC

8-86